Differentiation of superparamagnetic iron oxide nanoparticles and air pockets using independent component analysis

J. A. Langley[1,2], J. Lee[1,2], L. Wang[1,2], and Q. Zhao[1,2]
[1]Department of Physics & Astronomy, The University of Georgia, Athens, GA, United States, [2]Bioimaging Research Center, The University of Georgia, Athens, GA, United States

INTRODUCTION

Contrast agents based on superparamagnetic iron oxide nanoparticles (SPIOs) generate large susceptibility gradients that cause dephasing and signal loss in and around regions containing large concentrations of SPIOs. However, it is difficult to distinguish signal voids from aggregations of SPIOs *in vivo*. A method that measures the susceptibility ratio from two MR images acquired with different field strengths has been proposed (1). The main drawback for this method is the use of multiple scanners (at least two). To overcome the limitation of the requirement for multiple scanners, a single scanner based post-processing method is presented in this abstract.

Much work has been done to generate positive contrast from the hypointensities generated by the SPIOs. Positive contrast methods can be broken into two categories: pulse sequence methods and post-processing algorithms. Both pulse sequence methods and post-processing methods use magnetic field inhomogeneities to generate positive contrast. Recently published post-processing positive contrast algorithms focus on mapping the phase or susceptibility gradients generated by the SPIOs (2,3). As seen in Fig. 1, neither the phase gradient mapping (PGM) algorithm nor the susceptibility gradient mapping (SGM) algorithm is able to distinguish signal voids from SPIOs. In this abstract, independent component analysis (ICA) is used to differentiate signal voids from SPIOs. ICA has been used on many MR applications, e.g. segmentation of gray matter, white matter, and cerebral spinal fluid in the human brain (4). When used in tandem with a positive contrast method, the method will be able to distinguish SPIOs from signal voids.

THEORY

Three images were used in this analysis and are represented as $\mathbf{X} = [x_1,x_2,x_3]^T$ where x_i denotes a voxel vector in an MR image. Each image was acquired using differing TE and TR. ICA requires x_i to be a vector with zero mean so the mean value of x_i was subtracted from x_i. The voxels in each image are considered to be mixed signals depending on the transverse (T_1) and longitudinal relaxation times (T_2). $\mathbf{X}$ is assumed to be a combination of the three independent source signals originating from each voxel with $\mathbf{S} = [s_1,s_2,s_3]^T$ where s_i denotes the unmixed signals. ICA seeks an unmixing matrix $\mathbf{W}$ such that $\mathbf{S}=\mathbf{WX}$. The matrix $\mathbf{W}$ is calculated to make the components of $\mathbf{S}$ as independent as possible. The fastICA algorithm using negentropy was used in this abstract (5).

MATERIALS AND METHODS

An agar phantom was created to test the proposed method. Two vials were embedded within the agar phantom; one containing a solution with concentration 200 μg/ml of SPIOs (10 mn Fe_3O_4 nanocrystals, NN Labs, Fayetteville, AR) and the other vial was empty. Three images with different scan parameters were acquired on a 3.0 T GE Signa HDX MR Scanner (GE Medical Systems, Milwaukee, WI). The scan parameters for the first image were: time of repetition (TR) = 150 ms; echo time (TE) = 7 ms; bandwidth = 31.25KHz; number of excitations (NEX) = 1; matrix size = 128 x 128; field of view (FOV) = 11 cm; number of slices = 1; and slice thickness = 3 mm. The scan parameters for the second image were: TR = 250 ms; TE = 10 ms; bandwidth = 31.25KHz; NEX = 1; matrix size = 128 x 128; FOV = 11 cm; number of slices = 1; and slice thickness = 3 mm. The scan parameters for the third image were: TR = 500 ms; TE = 12 ms; bandwidth = 31.25KHz; NEX = 1; matrix size = 128 x 128; FOV = 11 cm; number of slices = 1; and slice thickness = 3 mm.

The fastICA algorithm, PGM method (2) and the SGM algorithm (3) were implemented in MATLAB (the MathWorks, Natick, Massachusetts). A Hamming window was applied to phase gradient calculated presented in (2) to reduce Gibbs ringing in the phase gradient.

RESULTS AND DISCUSSION

The difficulty in differentiating the vial with SPIOs, labeled 1, and the empty vial, labeled 2, is illustrated in Fig. 1. In magnitude image, Fig. 1a, both vials show a signal void. Both SGM and PGM utilize the phase map, shown in Fig. 1b, to generate positive contrast. As with the magnitude image, we are unable to differentiate either vial in the SGM map (Fig. 1c) and the PGM map (Fig. 1d). It can be seen, in Fig. 2, the contrast for the vial containing SPIOs has different contrast from that of the empty vial. To illustrate the effectiveness of the differentiation procedure, a map of the standard deviation, calculated by sliding a 2 x 2 box across the image, was created from the map of the first estimated signal y_1. The average of the standard deviation map for $y1$, $y2$, and $y3$ is shown in Fig. 2d. As expected, standard deviation the 2 x 2 box within the empty vial mimic the values of the background outside the phantom. Where as the standard deviations within the vial containing SPIOs is relatively uniform.

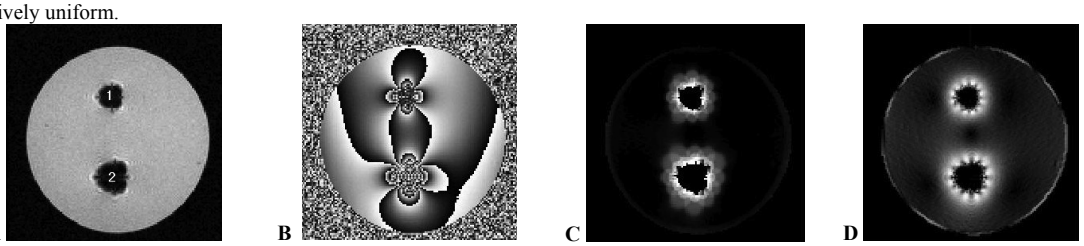

Figure 1. **a:** The magnitude image of the phantom data set. **b:** The phase map of the phantom data set. The SGM map and PGM map are shown in **c** and **d**, respectively. In **a**, the vial with SPIOs and empty vial are labeled as 1 and 2, respectively

In the linear mixing and unmixing model three assumptions are made: the number of sensors must be greater than or equal to the number of sources, the sources $s(t)$ must be mutually independent, and sensor noise must be negligible. In low SNR environments, where noise cannot be assumed to be negligible, the ICA method will not yield accurate results. In this abstract, we assume the number of sensors corresponds to three acquisitions with different combinations of TE and TR parameters. Hence, each voxel with longitudinal and transverse relaxation times will behave as a signal source. In this abstract, a relatively simple phantom containing three tissue types: agar gel, SPIO nanoparticles, and an empty vial was used. *In vivo* data sets are more complex than the phantom data set and will likely contain more tissue types. For *in vivo* data sets, more images will be needed to fully resolve the different tissue types.

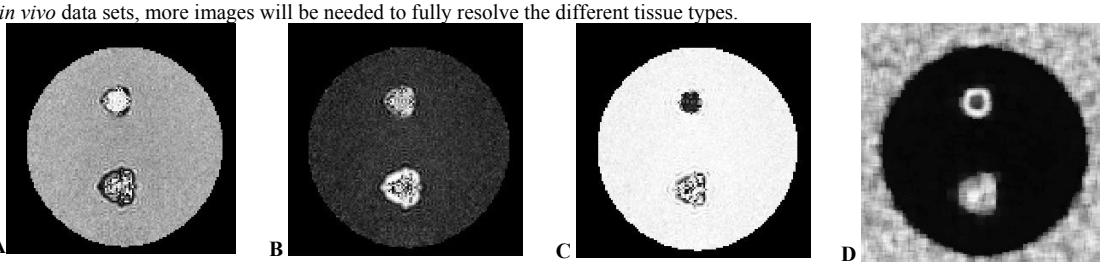

Figure 2. The results of the ICA analysis on the phantom data set. **a:** A map of the first estimated signal, y_1. **b:** The map of the second estimated signal y_2 and **c**: a map of the third estimated signal y_3 **d:** The mean of the map of the standard deviation of a 2 x 2 sliding box for **a**, **b**, and **c**.

In summary, ICA is able to differentiate a signal void from a vial containing SPIOs. Future studies will focus on applying this technique to *in vivo* data sets.

REFERENCES (1) Liu, MRI 28:1383 (2) Zhao, NMR Biomed *In Press* (DOI: 10.1002/nbm.1608) (3) Liu, NMR Biomed 21:242 (4) Chai, JMRI 32:24 (5) Hyvärinen, IEEE Neur Net 10:626

Acknowledgement: This work was supported by the John and Mary Franklin Foundation Paul D. Coverdell Neuroimaging Training Program